$$\frac{d[H\cdot]}{dt} = -(k_2[O_2] + a_2)[H\cdot] + k_1[H\cdot][OH\cdot] + k_3[H_2][O\cdot]$$

$$\frac{d[OH\cdot]}{dt} = k_2[O_2][H\cdot] - (k_1[H_2] + a_1)[OH\cdot] + k_3[H_2][O\cdot]$$

$$\frac{d[O\cdot]}{dt} = k_2[O\cdot][H\cdot] - (k_3[H\cdot] + a_3)[O\cdot]$$

until $[O_2] < k_2H_2(0)/k_3$, then with those conditions

Step 5

Use

$$\frac{d[OH\cdot]}{dt} = -a_1[OH\cdot]$$

$$\frac{d[H\cdot]}{dt} = -a_2[H\cdot]$$

$$\frac{d[O\cdot]}{dt} = -a_3[O\cdot]$$

until the desired time interval is completed. Use of such a five step scheme results in a very substantial savings in computation time with a small loss in accuracy.

Manuscript received May 12, 1981; revision received August 24, and accepted August 31, 1981

Viscoelastic Flow from a Tube into a Radial Slit

The viscoelastic flow from a tube into a radial slit between two parallel disks is investigated numerically by orthogonal collocation. A modified ZFD model and a generalized Newtonian fluid, with identical viscosity functions, are investigated. Results for these models indicate that fluid elasticity alters the velocity profiles significantly, but has little effect on the pressure profile in the radial flow region.

ALBERT CO

Department of Chemical Engineering and Rheology Research Center
Department of Chemical Engineering
University of Wisconsin
Madison, WI 53706

W. E. STEWART

Department of Chemical Engineering
University of Wisconsin
Madison, WI 53706

SCOPE

In steady shear flows, polymeric fluids are satisfactorily described by the Criminale-Ericksen-Filbey equation (Criminale et al., 1958; Ericksen, 1960; Bird et al., 1977), in which the viscometric functions (i.e., the viscosity and the primary and secondary normal stress coefficients) are the only material functions used. Aside from steady shear flows, the questions regarding the "proper" rheological equation of state and the required material functions are still unresolved.

Among the nonviscometric flows, converging-diverging flows are frequently encountered in polymer processing. This investigation focuses on a particular diverging flow, namely, the outward radial flow between two parallel disks, with the fluid introduced through a central tube. We describe the flow system, including the entrance region, by using an "appropriate" rheological model, whose parameters can be determined from available measurements of material functions, and by numerically solving the resulting system of nonlinear partial differential equations.

The principal rheological model used in the study is a modified Zaremba-Fromm-DeWitt (MZFD) model, which has six material parameters. The parameters are obtained from experimental data on the viscosity and primary normal stress coefficient for the given fluid.

In order to obtain a well-posed problem, the entry tube is extended to infinity, at which position the flow is considered to be fully developed. The radii of the disks are assumed equal and infinite, so that the Newtonian creeping-flow solution holds at the system outlet.

The numerical calculations are done by orthogonal collocation, in which the stream function, the shear stress and the two normal-stress differences are approximated by trial functions. Interior collocation points are chosen to be the zeros of the Tschebysheff and related polynomials. The system is divided into three regions, designated as the tube flow, stagnation flow, and radial flow regions. The trial functions are matched, at the junctions of these regions, by mass and momentum conservation conditions. The vorticity equation and the rheological equation of state are solved at the collocation points by a modified Newton method.

Correspondence concerning this paper should be addressed to A. Co, Department of Chemical Engineering, University of Wisconsin, Madison, WI 53706.
0001-1541-82-5765-0644-$2.00.

CONCLUSIONS AND SIGNIFICANCE

The parameters in the MZFD model are determined here for the Separan solution used in the radial flow experiments of Lee and Williams (1976b). The effect of elasticity is assessed by comparing the numerical results at Re $\approx 10^{-3}$ for the MZFD model with those for a generalized Newtonian fluid (GNF) that has the same viscosity function. In the tube and stagnation flow regions, the MZFD model gives a secondary peak in the velocity profile, whereas the GNF does not. At the inlet to the radial flow region, the velocity profile is practically symmetric for the GNF but strongly asymmetric for the MZFD model, and the pressure gradient for the MZFD model is higher than that for the GNF. At large values of r/r_0, the elastic effects become unimportant, and the MZFD radial velocity and radial pressure gradient in the radial flow region are in good agreement with those for the GNF. The MZFD and GNF predictions for the pressure profile at the lower disk are indistinguishable, but are slightly higher than the analytical result for a power-law fluid. The pressure profile data of Lee and Williams (1976b) lie above our model predictions. Because present experimental data are limited, this discrepancy cannot be explained at this time.

INTRODUCTION

Here we examine the flow of a viscoelastic fluid from a central tube into a radial slit between two parallel disks. Purely viscous fluids are considered elsewhere (Co, 1981).

The tube-and-disk flow system is represented schematically in Figure 1. The fluid enters the system at a constant flow rate through the tube connected to the upper disk, and then flows radially outward in the gap between the two parallel disks. The disks have an outer radius r_1, and the gap width is 2h. The circular tube has an inner radius r_0.

Theoretical studies of the steady viscoelastic radial flow are summarized in Table 1. These theoretical studies dealt primarily with the radial flow between the parallel disks and did not consider the flow in the tube nor in the stagnation region. The only exception is the work of Holstein and Paddon (1980) on an upper convected Maxwell model, which is characterized by a single relaxation time and a constant viscosity.

In the experimental studies cited in Table 2, the fluid flow rate was maintained at a steady value, and pressures were measured at various radial positions on the upper or lower disk. Dye tracer experiments with view perpendicular to the disks were also performed in some investigations. Note that in these experiments r_1/r_0 is about 10 and r_1/h ranges from 35 to 11,000.

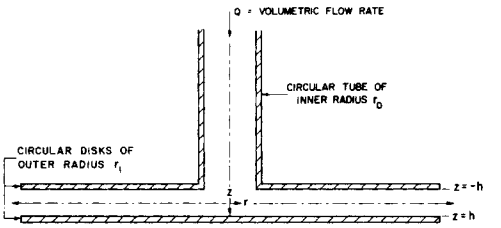

Figure 1. Tube and disk flow geometry ($r_1 \gg h$).

This flow system is of interest for the following reasons. (1) It can be used to evaluate rheological models, since the field is both sheared and stretched in this flow fluid. (2) It can be used as a viscometer to measure the zero-shear-rate viscosity (Schwarz and Bruce, 1969) and the second-order constants (Co and Bird, 1977). (3) It has applications in the design of air diffusers (which involve Newtonian fluids) and hydrostatic bearings (Woolard, 1957). (4) It resembles the arrangement in injection molding. However, it should be emphasized that this investigation deals only with isothermal steady radial flow. Mold filling, which is transient and non-isothermal, is not considered in this work.

TABLE 1. THEORETICAL STUDIES OF STEADY VISCOELASTIC RADIAL FLOW

Researcher	Fluid Model	Method of Solution	Fluid Inertia
Piau and Piau (1967, 1970)[1]	Second-Order Fluid	Series Expansion	Neglected
Schwarz and Bruce (1969)	Third-Order Fluid	"	Included
Lee and Williams (1976a)	Five-Constant Oldroyd	"	"
Co and Bird (1977)[1,2]	Third-Order Fluid	"	"
Holstein and Paddon (1980)[1,3]	Upper Convected Maxwell Model	Numerical	"

[1] No comparisons with experimental data were made.
[2] Co and Bird (1977) give the most detailed series expansion. Their results simplify to the earlier expressions obtained by Piau and Piau, Schwarz and Bruce, and Lee and Williams.
[3] Flow in the tube and in the stagnation region were included.

EQUATIONS OF CHANGE

In this investigation, the following assumptions are made. (1) The flow has reached steady state. (2) The fluid is incompressible, i.e., its density is constant. (3) The flow is symmetrical around the z-axis; hence, all variables are independent of the θ-coordinate. (4) There is no fluid motion in the θ-direction, i.e., $v_\theta = 0$. (5) Viscous heating is negligible and the flow remains isothermal. (6) No phase change occurs.

Since the flow is assumed to be axisymmetric, the velocity components can be expressed as derivatives of a stream function ψ (Bird et al., 1960), that is:

$$v_r = + (1/r)(\partial\psi/\partial z) \tag{1}$$

TABLE 2. EXPERIMENTAL STUDIES OF STEADY VISCOELASTIC RADIAL FLOW

Researcher	Fluids Studied	r_1/h	r_1/r_0
Schwarz and Bruce (1969)	Polyacrylamide Solutions	880–10,700	10
Laurencena and Williams (1974)[1]	Carboxy-Polymethylene Solutions, Hydroxyethyl Cellulose Solution	600–2,600	10
Winter (1975)	Low and High Density Polyethylenes, Polystyrene	35–170	20
Lee and Williams (1976b)[1]	Polyacrylamide Solutions	440–1,400	10
Amadou, Alder and Piau (1978)[2]	Polyethylene Oxide Solutions	970–2,550	30

[1] Tracer experiments with view perpendicular to the disks were also performed.
[2] This work deals with converging radial flow.

$$v_z = -(1/r)(\partial\psi/\partial r) \tag{2}$$

The above equations automatically satisfy the equation of continuity for an incompressible fluid, i.e., $(\nabla\cdot v) = 0$.

For incompressible fluids, the conservation of momentum gives:

$$\rho D\,v/Dt = -\nabla\mathcal{P} - [\nabla\cdot\tau] \tag{3}$$

Here, the gravitational forces are incorporated in the modified pressure $\mathcal{P}$. Taking the curl of this equation, one gets the vorticity equation:

$$[\nabla\times\rho D\,v/Dt] = -[\nabla\times[\nabla\cdot\tau]] \tag{4}$$

The pressure term drops out since the curl of the gradient of a scalar field is zero.

Modified ZFD Model (MZFD)

To describe the stress-strain relations of viscoelastic fluids, we use the constitutive equation:

$$\tau + \lambda(\mathcal{D}\tau/\mathcal{D}t) = -\eta(1 + \lambda^2\dot\gamma^2\dot\gamma \tag{5}$$

Equation 5 is a modification by Co (1979) of the ZFD (corotational Maxwell) model proposed by Zaremba (1903), Fromm (1947, 1948) and DeWitt (1955). Here the viscosity η and the fluid characteristic time λ depend on the scalar invariant $\dot\gamma \equiv \sqrt{(1/2)(\dot\gamma:\dot\gamma)}$. In addition, the $\dot\gamma$ term is multiplied by the quantity $(1 + \lambda^2\dot\gamma^2)$. The material functions for this model are summarized in Table 3, and their derivations are given in Co (1979). If $\lambda = 0$, this model reduces to the generalized Newtonian fluid (GNF).

To describe the shear-thinning viscosity, we use the Carreau viscosity function (Carreau, 1968):

$$\eta = \eta_0\,(1 + \lambda_v^2\dot\gamma^2)^{(n-1)/2} \tag{6}$$

At high $\dot\gamma$, Eq. 6 reduces to the power law $\eta = m\dot\gamma^{n-1}$ with $m = \eta_0\lambda_v{}^{n-1}$. For the fluid characteristic time, we use

$$\lambda = \lambda_0(1 + \lambda_t^2\dot\gamma^2)^{(\bar n)-1)/2} \tag{7}$$

With these assumed forms for η and λ, the model has six material constants. The constants η_0, λ_v and n are determined by curve-fitting viscosity data, and the constants λ_0, λ_t and $\bar n$ are found by curve-fitting normal-stress data.

Some sample model parameters are shown in Table 4. These parameters describe a solution consisting of 1.0% nonionic polyacrylamide (Separan NP 10, Dow Chemical), 49.5% glycerine, and 49.5% water, used by Lee and Williams (1976b) in their radial-flow experiments. These parameters were determined from the viscosity and normal-stress data of Lee and Williams (1976b), obtained in a Weissenberg Rheogoniometer R-17 with a cone-and-plate geometry of cone angle 0.5° and diameter 10 cm. They measured

TABLE 4. MODEL PARAMETERS FOR LEE-WILLIAMS SEPARAN SOLUTION

η_0 [Pa·s]	23.7
λ_v [s]	38.29
λ_0 [s]	1.428
λ_t [s]	27.72
n	0.4741
$\bar n$	0.423
Λ_v	817.7
Λ_0	30.50
Λ_t	592.0

The dimensionless time constants are calculated with

$$\rho = 1.14\times10^3\ \text{kg/m}^3$$

$$r_0 = 3.12\times10^{-2}\ \text{m}$$

The experimental data for η and Ψ_1 can be found in Lee and Williams (1976b).

TABLE 3. MATERIAL FUNCTIONS FOR MODIFIED ZFD MODEL (EQ. 5)

Experiments	Material Functions	
Steady-State Shear Flow	$\eta(\dot\gamma)$	$\equiv -\tau_{yx}/\dot\gamma$, where $\eta(\dot\gamma)$ is arbitrary (A)
$v_x = \dot\gamma y$	$\Psi_1(\dot\gamma)$	$\equiv -(\tau_{xx} - \tau_{yy})/\dot\gamma^2 = 2\lambda(\dot\gamma)\eta(\dot\gamma)$, where $\lambda(\dot\gamma)$ is arbitrary (B)
	$\Psi_2(\dot\gamma)$	$\equiv -(\tau_{yy} - \tau_{zz})/\dot\gamma^2 = -\Psi_1/2$ (C)
Stress Growth after Sudden Inception of Steady Shear Flow $v_x = \dot\gamma_0 y$ at $t = 0$	$\eta^+(t;\dot\gamma_0)$	$\equiv -\tau_{yx}(t)/\dot\gamma_0$
		$\equiv \eta(\dot\gamma_0)\{1\text{-exp}[-t/\lambda(\dot\gamma_0)]\,[\cos(\dot\gamma_0 t) - \lambda(\dot\gamma_0)\dot\gamma_0\sin(\dot\gamma_0 t)]\}$ (D)
	$\Psi_1^+(t;\dot\gamma_0)$	$\equiv -[\tau_{xx}(t) - \tau_{yy}(t)]/\dot\gamma_0^2$
		$\equiv \Psi_1(\dot\gamma_0)\{1\text{-exp}[-t/\lambda(\dot\gamma_0)]\,[\cos(\dot\gamma_0 t) + \sin(\dot\gamma_0 t)/(\lambda(\dot\gamma_0)\dot\gamma_0)]\}$ (E)
	$\Psi_2^+(t;\dot\gamma_0)$	$\equiv -[\tau_{yy}(t) - \tau_{zz}(t)]/\dot\gamma_0^2 = -\Psi_1^+(t;\dot\gamma_0)/2$ (F)
	$\eta^-(t;\dot\gamma_0)$	$\equiv -\tau_{xy}(t)/\dot\gamma_0 = \eta(\dot\gamma_0)\exp(-t/\lambda_0)$ (G)
		where λ_0 denotes $\lambda(0)$
Stress Relaxation after Sudden Cessation of Steady Shear Flow $v_x = \dot\gamma_0 y$ at $t = 0$	$\Psi_1^-(t;\dot\gamma_0)$	$\equiv -[\tau_{xx}(t) - \tau_{yy}(t)]/\dot\gamma_0^2 = \Psi_1(\dot\gamma_0)\exp(-t/\lambda_0)$ (H)
	$\Psi_2^-(t;\dot\gamma_0)$	$\equiv -[\tau_{yy}(t) - \tau_{zz}(t)]/\dot\gamma_0^2 = -\Psi_1^-(t;\dot\gamma_0)/2$ (I)
Steady Elongational Flow $v_z = \dot\epsilon z$ $v_x = -\dot\epsilon x/2$ $v_y = -\dot\epsilon y/2$	$\bar\eta(\dot\epsilon)$	$\equiv -(\tau_{zz} - \tau_{xx})/\dot\epsilon$ (J)
		$\equiv 3\,\eta(\sqrt{3}\dot\epsilon)\,[1 + 3\,\lambda^2\,(\sqrt{3}\dot\epsilon)\dot\epsilon^2]$
	(See Fig. 3)	
Elongational Stress Growth after Sudden Inception of Steady Elongational Flow at $t = 0$ $v_z = \dot\epsilon_0 z$ $v_x = -\dot\epsilon_0 x/2$ $v_y = -\dot\epsilon_0 y/2$	$\bar\eta^+(t;\dot\epsilon_0)$	$\equiv -[\tau_{zz}(t) - \tau_{xx}(t)]/\dot\epsilon_0$ (K)
		$\equiv \bar\eta(\sqrt{3}\dot\epsilon_0)\,\{1 - \exp[-t/\lambda(\sqrt{3}\dot\epsilon_0)]\}$

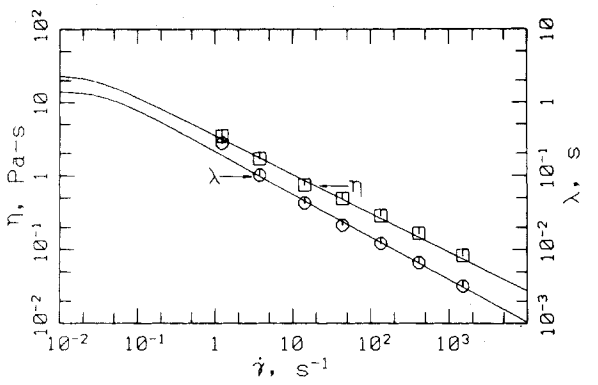

Figure 2. Dependence of viscosity η and fluid characteristic time $\lambda = \Psi 1/2\ \eta$ on shear rate $\dot{\gamma}$ for Lee-Williams Separan solution. The solid lines represent model predictions using parameters in Table 4. Data are from Lee and Williams (1976b). The definition for λ used here is different from that used in Lee and Williams.

the zero-shear-rate viscosity by the falling-ball method. The fitted curves for η and λ ($= \Psi_1/2\eta$), together with the experimental data, are shown in Figure 2. The parameter λ_0 was estimated by extrapolation, assuming the ratio η/λ to be constant. This extrapolation is unimportant in the present calculations, since our solutions for $\dot{\gamma}$ at the grid points all fall within the power law region of Figure 2.

Since the fluid is stretched as it flows outward from the tube, an appropriate rheological model must give a satisfactory description of the elongated viscosity. To check this, we used the parameters in Table 4 to predict the elongational viscosity curve in Figure 3. The predicted curve for $\dot{\epsilon} < 30s^{-1}$ does have a shape similar to kinetic theory predictions of $\bar{\eta}$ for melts (Doi and Edwards, 1979; Curtiss and Bird, 1981). Moreover, solution data by Pearson and Middleman (1977) showed $\bar{\eta}$ decreasing with increasing $\dot{\epsilon}$. The following calculations all fall in the downward-sloping region of Figure 3, and are thus unaffected by the upturn of our $\bar{\eta}$ function at $\dot{\epsilon} \approx 30s^{-1}$.

Dimensionless Differential Equations

To transform the basic equations into dimensionless form, we introduce the following dimensionless variables:

$$R = r/r_0;\ Z = z/h;\ \Psi = 2\pi(\psi - \psi^o)/Q \qquad (8,9,10)$$

$$\Omega = 2\pi r_0 h^2 \omega/Q;\ T = 2\pi_0 h^2 \tau_{rz}/\eta_0 Q \qquad (11,12)$$

$$M = 2\pi r_0 h^2(\tau_{zz} - \tau_{\theta\theta})/\eta_0 Q;\ N = 2\pi r_0 h^2(\tau_{rr} - \tau_{\theta\theta})\eta_0 Q \qquad (13,14)$$

$$\dot{\Gamma} = 2\pi r_0 h^2 \dot{\gamma}/Q;\ H = \eta/\eta_0;\ \Lambda = \lambda\eta_0/\rho r_0^2 \qquad (15,16,17)$$

and the following dimensionless groups:

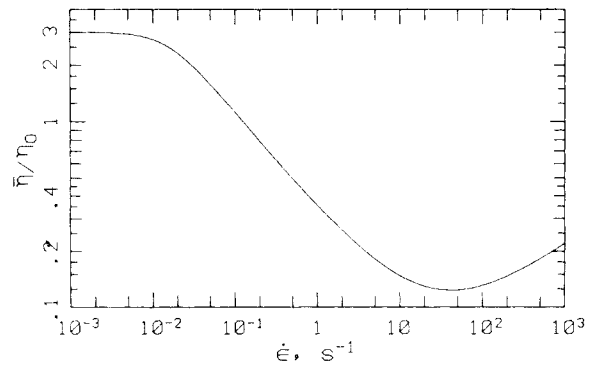

Figure 3. Dependence of elongational viscosity $\bar{\eta}$ on elongational rate $\dot{\epsilon}$ for the Lee-Williams Separan solution. The solid lines represent model predictions using parameters from Table 4.

$$R_0 = r_0/h;\ \mathrm{Re} = 2\rho Q/\pi r_0 \eta_0 \qquad (18,19)$$

$$\Lambda_0 = \eta_0\lambda_0/\rho r_0^2;\ \Lambda_t = \eta_0\lambda_t/\rho r_0^2;\ \Lambda_v = \eta_0\lambda_v/\rho r_0^2 \qquad (20,21,22)$$

The resulting dimensionless equations are summarized in Table 5.

Equations A to D of Table 5 are solved simultaneously for Ψ, T, M and N. After these functions have been computed, the radial component of the equation of motion (Eq. E of Table 5) is used to obtain the gradient $\partial P/\partial R$, in which P is defined as

$$P = 2\pi r_0 h^2[\mathcal{P} + \tau_{zz}) - (\mathcal{P} + \tau_{zz})^o]/\eta_0 Q \qquad (23)$$

and vanishes at a reference position ($R = R^o$, $Z = Z^o$). With R^o specified, one can then integrate the computed $\partial P/\partial R$ to get the P distribution at $Z = Z^o$.

BOUNDARY CONDITIONS

In order to obtain a well-posed, realistic problem statement, we include the inlet tube in the analysis and make the following assumptions:

1. The tube is sufficiently long so that at some distance from the inlet to the parallel disks, the flow is fully developed.
2. The exit effects at the outer edge of the parallel disks are negligible. This is a reasonable assumption since the ratio r_1/h is rather large in the experiments on this flow system (Table 2).
3. The tube is connected to the upper disk with a square edge (Figure 1).

Using the first assumption, we extend the tube to infinity and use the fully-developed tube flow conditions as the boundary conditions at $-1/Z = 0$. Using the second assumption, we extend the parallel disks to infinity and use the Newtonian creeping-flow solutions as the boundary conditions at $1/R = 0$.

The boundary conditions used are summarized in Table 6. Here we have used the stream function at the tube wall and upper disk as the reference value ψ^o.

ORTHOGONAL COLLOCATION

The system of partial differential equations is solved by orthogonal collocation. Detailed descriptions and applications of this technique are given in Villadsen and Stewart (1967); Nirschl (1971); Finlayson (1972); Sørensen (1972); Sørensen, Guertin, and Stewart (1973); Sørensen, Willis, and Stewart (1973); Sørensen and Stewart (1974); Guertin et al. (1977); Stewart et al. (1978); Villadsen and Michelsen (1978); and Chang et al. (1979).

The radial flow system can be divided into three flow regions, as shown in Figure 4. Each variable is approximated by a different trial function in each region. At the junctions of the regions, these trial functions should satsify the conditions summarized in Table 7. The derivation of these matching conditions is given in Co (1979).

The trial functions used in this investigation are summarized in Table 8. We have written the trial functions for the stream function as

$$(\Psi)_i = \Psi_i^o + \Psi_i^c\ (i = 1, 2, 3) \qquad (24)$$

where the Ψ_i^o are known functions that satisfy the boundary conditions of Table 6 and Eqs. A and E in Table 7. Note that Ψ_1^o and Ψ_3^o are the solutions for Newtonian fully-developed tube flow and Newtonian creeping radial flow, respectively. Since we have chosen the Ψ_i^o to satisfy the boundary conditions for $(\Psi)_i$, all the boundary conditions for the Ψ_i^o are homogeneous.

The order of each trial expansion Ψ_i is defined by the number of collocation points. The numbers of collocation points in the three flow regions are interrelated as shown in Table 9. In each flow region, the interior collocation points are taken as the zeros of the polynomials shown in Table 10. Numerical values of the zeros of these polynomials for various degrees are given in Table 11. The arrangement of the collocation points is illustrated in Figure 4 for the case $NRT1 = 3$, $NRT3 = 3$, $NZT1 = 3$, and $NZT3 = 4$.

TABLE 5. DIFFERENTIAL EQUATIONS FOR STEADY FLOW IN TUBE-DISK SYSTEM

Vorticity:	$(1/R_0)(\partial(1/R)\partial(RT)/\partial R] + \partial^2 M/\partial R\partial Z - (1/R)(\partial^2(RN)/\partial R\partial Z) - R_0(\partial^2 T/\partial Z^2) - (\mathrm{Re}/4)[(\partial(\Omega/R)/\partial R)(\partial\Psi/\partial Z)$ $- (1/R)(\partial\Psi/\partial R)(\partial\Psi/\partial Z)] \equiv 0$	(A)
Stresses:	$T + (\mathrm{Re}R_0\Lambda/4)(1/R)[(\partial\Psi/\partial Z)(\partial T/\partial R) - (\partial\Psi/\partial R)(\partial T/\partial Z)] + (\mathrm{Re}R_0^2\Lambda/8)\Omega(N - M) + \mathrm{H}[1 + (\mathrm{Re}R_0^2\Lambda/4)^2\dot{\Gamma}^2](1/R)(\partial^2\Psi/\partial Z^2)$ $- (1/R_0^2)(\partial[(1/R)(\partial\Psi/\partial R)]/\partial R)] \equiv 0$	(B)
	$M + (\mathrm{Re}R_0\Lambda/4)(1/R)[(\partial\Psi/\partial Z)(\partial M/\partial R) - (\partial\Psi/\partial R)(\partial M/\partial Z)] + (\mathrm{Re}R_0^2\Lambda/4)\,\Omega T - (2/R_0)\mathrm{H}[1 + (\mathrm{Re}R_0^2\Lambda/4)^2\dot{\Gamma}^2](1/R)(\partial^2\Psi/\partial R\partial Z)$ $+ (1/R^2)(\partial\Psi/\partial Z)] \equiv 0$	(C)
	$N + (\mathrm{Re}R_0\Lambda/4)(1/R)[(\partial\Psi/\partial Z)(\partial N/\partial R) - (\partial\Psi/\partial R)(\partial N/\partial Z)] - (\mathrm{Re}R_0^2\Lambda/4)\Omega T + (2/R_0)\mathrm{H}[1 + (\mathrm{Re}R_0^2\Lambda/4)^2\dot{\Gamma}^2](1/R)(\partial^2\Psi/\partial R\partial Z)$ $- (2/R^2)(\partial\Psi/\partial Z)] \equiv 0$	(D)
Motion:	$\partial P/\partial R = \partial M/\partial R - (1/R)(\partial(RN)/\partial R) - R_0(\partial T/\partial Z) - (\mathrm{Re}/4)(1/R^2)[(\partial\Psi/\partial Z)(\partial^2\Psi/\partial R\partial Z - (1/R)(\partial\Psi/\partial Z)) - (\partial\Psi/\partial R)(\partial^2\Psi/\partial Z^2)]$	(E)
(R-Component)		
The dimensionless variables Ω, $\dot{\Gamma}^2$, H and Λ are determined by:		
$\Omega \equiv (1/R_0^2)(\partial[(1/R)(\partial\Psi/\partial R)]/\partial R) + (1/R)(\partial^2\Psi/\partial Z^2)$		(F)
$\dot{\Gamma}^2 \equiv [(1/R)(\partial^2\Psi/\partial Z^2) - (1/R_0^2)(\partial[(1/R)(\partial\Psi/\partial R)]/\partial R)]^2 + (4/R_0^2)[(1/R^2)(\partial^2\Psi/\partial R\partial Z)^2$ $-(1/R^3)(\partial\Psi/\partial Z)(\partial^2\Psi/\partial R\partial Z) + (1/R^4)(\partial\Psi/\partial Z)^2]$		(G)
$\mathrm{H} \equiv [1 + (\mathrm{Re}R_0^2\Lambda_0/4)^2\dot{\Gamma}^2]^{(n-1)/2}$		(H)
$\Lambda = \Lambda_0[1 + (\mathrm{Re}R_0^2\Lambda_1/4)^2\dot{\Gamma}^2]^{(n-1)/2}$		(I)

TABLE 6. BOUNDARY CONDITIONS FOR DISK-TUBE SYSTEM

At Tube Wall	$(R = 1; -1 \le 1/Z \le 0)$:	
	$\Psi = 0$	(A)
	$\partial\Psi/\partial R = 0$ (No-Slip Condition)	(B)
At Axis	$(R = 0; Z \le 1)$	
	$\Psi = 1$	(C)
	$\partial[(1/R)(\partial\Psi/\partial R)]/\partial R = 0$ (Symmetry)	(D)
At Upper Disk	$(0 \le 1/R \le 1; Z = -1)$	
	$\Psi = 0$	(E)
	$\partial\Psi/\partial Z = 0$ (No-Slip Condition)	(F)
At Lower Disk	$(R \ge 0; Z = 1)$	
	$\Psi = 1$	(G)
	$\partial\Psi/\partial Z = 0$ (No-Slip Condition)	(H)
At (Infinite) Tube Inlet	$(0 \le R \le 1; -1/Z = 0)$	
	$\partial\Psi/\partial Z = 0$; $\partial T/\partial Z = 0$	(I,J)
	$\partial M/\partial Z = 0$; $\partial N/\partial Z = 0$	(K,L)
	(Fully Developed Tube Flow)	
At (Infinite) Disk Outlet	$(1/R = 0; -1 \le Z \le 1)$	
	$\Psi = (2 + 3Z - Z^3)/4$	(M)
	$T = 0$; $M = 0$; $N = 0$	(N,O,P)
	(Newtonian Creeping Flow)	

In Table 9, we see that the numbers of collocation points for the variables in the three flow regions are defined if we specify $NRT1$, $NRT3$, $NZT1$, and $NZT3$. The collocation points for the stream function and stresses are related through their corresponding polynomials shown in Table 10. The collocation points in the R-coordinate in regions 1 and 2 are related because the expansions Ψ_1^c and Ψ_2^c must be of the same order in R to satisfy (Eq. A of Table 7). The same can be said for the Z-coordinate in regions 2 and 3 to satisfy (Eq. E of Table 7).

As shown in Table 10, we use the Tschebysheff polynomial $T_n(x)$ [in which $-1 \le x \le 1$] and the shifted Tschebysheff polynomial $T_n^*(x)$ [in which $0 \le x \le 1$] to determine the collocation points for the stresses. Descriptions of these polynomials can be found in texts in numerical analysis (for example, Lanczos, 1956; Ralston, 1965). It should be noted that of all polynomials of degree n with coefficient of x^n equal to unity, the Tschebysheff polynomial of degree n multiplied by $\frac{1}{2}^{n-1}$ has the least peak amplitudes on the interval $[-1,1]$. [See §7.5 in Ralston (1965) for proof of this theorem.] This property of $T_n(x)$ is of particular interest to us. The shifted Tschebysheff polynomial $T_n^*(x)$ has the same property on the interval $[0,1]$. If the variable x is changed to x^2, one can easily show that

$$T_n^*(x^2) = T_{2n}(x) \tag{25}$$

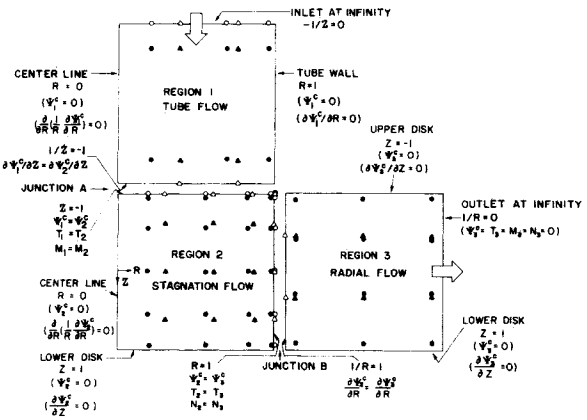

Figure 4. Typical arrangement of the collocation points. Here we show the stream function interior (▲) and boundary (△) points and the stress interior (●) and boundary (○) points for the case of $NRT1 = 3$, $NRT3 = 3$, $NZT1 = 3$, and $NZT3 = 4$. The boundary conditions, enclosed in parentheses, are exactly satisfied.

TABLE 7. MATCHING CONDITIONS AT JUNCTIONS OF FLOW REGIONS

At Junction A ($Z = -1$):

$(\Psi)_1 = (\Psi)_2$ (Conservation of Mass) (A)

$(\partial\Psi/\partial Z)_1 = (\partial\Psi/\partial Z)_2$ (Continuity of v_r) (B)

$(T)_1 = (T)_2$ (C)

(Conservation of Momentum)

$(M)_1 = (M)_2$ (D)

At Junction B ($R = 1$):

$(\Psi)_2 = (\Psi)_3$ (Conservation of Mass) (E)

$(\partial\Psi/\partial R)_2 = (\partial\Psi/\partial R)_3$ (Continuity of v_z) (F)

$(T)_2 = (T)_3$ (G)

(Conservation of Momentum)

$(N)_2 = (N)_3$ (H)

In the tube flow region (region 1), the shear stress T is expressible by expansion in the basis functions $RT_i^*(R^2)T_j^*(1-1/Z)$. Assuming good convergence of this expansion, the error in T will be dominated by the first omitted term, a multiple of $RT_{NRT1}^*(R^2)T_{NZT1-1}^*(-1/Z)$. The total error in approximation of the vorticity equation is then proportional to the product of $T_{NZT1-1}^*(-1/Z)$ and the polynomial

$$\phi_{NRT1-1}(R^2) = d[R^{-1}d[R^2T_{NRT1}^*(R^2)]/dR]dR \qquad (26)$$

TABLE 8. TRIAL FUNCTIONS FOR STREAM FUNCTION, STRESSES AND RADIAL PRESSURE GRADIENT

Region 1 (Tube Flow):

$\Psi_1^o = (1 - R^2)^2$ (A)

$$\Psi_1^c = R^2(1-R^2)^2 \sum_{j=1}^{NZV1}\sum_{i=1}^{NRV1} c_{\Psi,ij}^{[1]} R^{2i-2}Z^{1-j} \qquad (B)$$

$$T_1 = \sum_{j=1}^{NZT1}\sum_{i=1}^{NRT1} c_{T,ij}^{[1]} R^{2i-1}Z^{1-j} \qquad (C)$$

$$M_1 = \sum_{j=1}^{NZT1}\sum_{i=1}^{NRT1} c_{M,ij}^{[1]} R^{2i-1}Z^{1-j} \qquad (D)$$

$$N_1 = \sum_{j=1}^{NZT1}\sum_{i=1}^{NRT1} c_{N,ij}^{[1]} R^{2i-1}Z^{1-j} \qquad (E)$$

Region 2 (Stagnation Flow):

$\Psi_2^o = 1 - (1/4)R^2(1-Z)^2(2+ZR^2)$ (F)

$$\Psi_2^c = R^2(1-Z)^2 \sum_{j=1}^{NZV2}\sum_{i=1}^{NRV2} c_{\Psi,ij}^{[2]} R^{2i-2}Z^{j-1} \qquad (G)$$

$$T_2 = \sum_{j=1}^{NZT2}\sum_{i=1}^{NRT2} c_{T,ij}^{[2]} R^{2i-1}Z^{j-1} \qquad (H)$$

$$M_2 = \sum_{j=1}^{NZT2}\sum_{i=1}^{NRTD2} c_{M,ij}^{[2]} R^{2i-2}Z^{j-1} \qquad (I)$$

$$N_2 = \sum_{j=1}^{NZTD2}\sum_{i=1}^{NRT2} c_{N,ij}^{[2]} R^{2i-2}Z^{j-1} \qquad (J)$$

Region 3 (Radial Flow):

$\Psi_3^o = (2 + 3Z - Z^3)/4$ (K)

$$\Psi_3^c = (1-Z^2)^2 \sum_{j=1}^{NZV3}\sum_{i=1}^{NRV3} c_{\Psi,ij}^{[3]} R^{-i}Z^{j-1} \qquad (L)$$

$$T_3 = \sum_{j=1}^{NZT3}\sum_{i=1}^{NRT3} c_{T,ij}^{[3]} R^{-i}Z^{j-1} \qquad (M)$$

$$M_3 = \sum_{j=1}^{NZT3}\sum_{i=1}^{NRT3} c_{M,ij}^{[3]} R^{-i}Z^{j-1} \qquad (N)$$

$$N_3 = \sum_{j=1}^{NZT3}\sum_{i=1}^{NRT3} c_{N,ij}^{[3]} R^{-i}Z^{j-1} \qquad (O)$$

$$\partial P_3/\partial R = \sum_{j=1}^{NZT3}\sum_{i=1}^{NRT3} c_{P,ij}^{[3]} R^{-i}Z^{j-1} \qquad (P)$$

The upper indices in the summations are defined in Table 9.
The $c_{\Psi,ij}^{[1]}$ are the adjustable coefficients in the trial functions.

TABLE 9. SPECIFICATION OF NUMBERS OF COLLOCATION POINTS FOR STREAM FUNCTION STRESSES AND RADIAL PRESSURE GRADIENT

Trial Function	Number of Collocation Points: R-Coordinate	Number of Collocation Points: Z-Coordinate
Ψ_1^c	$NRV1 = NRT1 - 1$	$NZV1 = NZT1 + 1^{a,b}$
T_1, M_1, N_1	$NRT1$	$NZT1^a$
Ψ_1^c	$NRV2 = NRV1 + 2^d$	$NZV2 = NZV3 + 2^b$
T_2	$NRT2 = NRT1 + 2^d$	$NZT2 = NZT3 + 2^b$
M_2	$NRTD2 = NRT1 + 1$	$NZT2 = NZT3 + 2^b$
N_2	$NRT2 = NRT1 + 2^d$	$NZTD2 = NZT3 + 1$
Ψ_3^c	$NRV3 = NRT3 + 1^d$	$NZV3 = NZT3 - 2$
$T_3, M_3, N_3, \partial P_3/\partial R$	$NRT3$	$NZT3$

For the marked entries, the collocation points include points on the region boundary (Figure 4):

[a] $Z = -\infty$

[b] $Z = Z^{-1} = -1$

[d] $R = R^{-1} = 1$

if the corresponding stress derivative is a dominant term in the vorticity equation, as we assume. Accordingly, the error in T/R can be minimized in the Tschebysheff sense over the entire tube by collocating the vorticity equation at the intersections of the zeros of $\phi_{NRT1-1}(R^2)$ and $T_{NZT1-1}^*(-1/Z)$.

In the radial flow region (region 3), we can expand the shear stress T in the basis functions $T_i^*(1/R)T_j(Z)$. If this expansion has good convergence, the error in T will be a multiple of $T_{NZT3}^*(1/R)T_{NZT3}(Z)$. Assuming that the stress derivative $\partial^2T/\partial Z^2$ is a dominant term in the vorticity equation, the total errors in approximation of the vorticity equation is then proportional to the product of $T_{NRT3}^*(1/R)$ and the polynomial

$$\phi_{NZT3-2}(Z) = d^2T_{NZT3}(Z)/dZ^2 \qquad (27)$$

The error in T can then be minimized in the Tschebysheff sense over the radial flow region by collocating the vorticity equation at the intersections of the zeros of $T_{NRT3}^*(1/R)$ and $\phi_{NZT3-2}(Z)$.

In the stagnation flow region (region 2), the collocation points are chosen by following the same line of reasoning and by using Eqs. A and E of Table 7.

SOLUTION STRATEGY

To solve the complete steady-state radial flow problem, we first obtain the steady-state solution for fully-developed tube flow. The results for Ψ^c, T, M, and N are used as boundary values at the tube inlet ($-1/Z = 0$). The numerical method used to generate the fully-developed tube flow solution is similar to that described below

TABLE 10. POLYNOMIALS WHOSE ZEROS ARE USED AS INTERIOR COLLOCATION POINTS FOR STREAM FUNCTION, STRESSES AND RADIAL PRESSURE GRADIENT

Trial Function	Polynomial: R-Coordinate	Polynomial: Z-Coordinate
Ψ_1^c	$d[R^{-1}d[R^2T_{NRT1}^*(R^2)]/dR]/dR^a$	
T_1, M_1, N_1	$T_{NRT1}^*(R^2) = T_{2(NRT1)}(R)^a$	$T_{NZT1-1}^*(Z^{-1})^b$
Ψ_2^c	$d[R^{-1}d[R^2T_{NRTD2}^*(R^2)]/dR]/dR^a$	$d^2T_{NZTD2}(Z)/dZ^2$
T_2, M_2, N_2	$T_{NRTD2}^*(R^2) = T_{2(NRTD2)}(R)^a$	$T_{NZTD2}(Z)$
Ψ_3^c		$d^2T_{NZT3}(Z)/dZ^2$
$T_3, M_3, N_3, \partial P_3/\partial R$	$T_{NRT3}^*(R^{-1})$	$T_{NZT3}(Z)$

$T_n(x)$ represents the Tschebysheff polynomial of degree n in x, and $T_n^*(x)$, the shifted Tschebysheff polynomial of degree n in x. For the marked entries, the interior collocation points are:

[a] The positive zeros of the given polynomial.

[b] The negatives of the zeros of the given polynomial.

TABLE 11. ZEROS OF POLYNOMIALS

Degree	Tschebysheff[a]	Shifted Tschebysheff[b]	Eq. 26	Eq. 27
2	±0.70710678	0.14644661	0.39811261	±0.40824829
		0.85355339	0.77909450	
3	0.00000000	0.06698730	0.30219805	0.00000000
	±0.86602540	0.50000000	0.60926274	±0.61237244
		0.93301270	0.85876378	
4	±0.38268343	0.03806023	0.24311701	±0.26621648
	±0.92387953	0.30864828	0.50000000	±0.72741239
		0.69134172	0.73268828	
		0.96193977	0.90594076	
5	0.00000000	0.02447174	0.20321704	0.00000000
	±0.58778526	0.20610737	0.42249426	±0.44293046
	±0.95105652	0.50000000	0.63217153	±0.79821422
		0.79389263	0.80775195	
		0.97552826	0.93324943	

For the marked entries, the zeros can be calculated using:
[a] $x_i = \cos[\pi(2i-1)/2n]$
[b] $x_i = \cos^2[\pi(2i-1)/4n]$
in which $i = 1, 2, \ldots, n$.

for the complete system.

In each flow region of the complete system (Figure 4), the vorticity equation (Eq. A in Table 5) is applied at the interior collocation points for the stream function. The stress equations (Eqs. B–D in Table 5) are applied at the interior collocation points for the stresses. The matching conditions in Table 7 are applied at the junction points. The spatial derivatives in these equations are obtained by Lagrangian differentiation (also known as the method of ordinates; Villadsen and Stewart, 1967). To reduce the order of the resulting system of algebraic equations, we eliminate Ψ_2^c, T_2 and M_2 at junction A ($Z = -1$) by use of Eqs. A, C and D in Table 7 and eliminate Ψ_2^c, T_2 and N_2 at junction B ($R = 1$) by use of Eqs. E, G and H in Table 7. Equations B and F in Table 7 are applied at the junction collocation points for Ψ_1^c and Ψ_3^c, respectively.

The remaining equations are strictly nonlinear. They are solved by Newton's method with a line search to minimize the sum of squares of the residuals in each iteration. [See Co (1979) for details.] The Jacobian matrix required in Newton's method is obtained by differentiating the nonlinear algebraic equations *analytically*. The convergence of the numerical methods is discussed elsewhere (Co, 1979). The calculations were checked for convergence by varying the number of collocation points; the following results represent the finest grid.

RESULTS AND DISCUSSION

The velocity and pressure profiles for a *GNF* ($\Lambda_v = 817.7$, $n = 0.4741$, $\Lambda_0 = \Lambda_t = \bar{n} = 0$) are shown in Figures 5(a) to (e). Those for a MZFD model (with the parameters of Table 4) are given in Figures 6(a) to (e). Both cases have $\mathrm{Re} = 1.096 \times 10^{-3}$, $R_0 = 60$ and the same viscosity function. The only difference between the two cases lies in the fluid characteristic time λ.

The velocity profiles for the viscoelastic (MZFD) model in the tube flow and the stagnation flow regions [Figures 6(a) to (c)] differ strikingly from those for an inelastic fluid with the same viscosity function [Figures 5(a) to (c)]. Figure 6(a) shows the changes in the axial velocity profile in viscoelastic flow as the fluid approaches the tube outlet. These changes in shape are apparently caused by viscoelastic responses propagating upstream from the corner region. A new velocity peak appears near the corner [Figure 6(a)] in the viscoelastic flow and persists into the stagnation flow region [Figures 6(b) and (c)]. Co (1981) obtained a qualitatively similar velocity peak near the corner for Newtonian flow at Re = 100; however, the peak in that case was due to fluid inertia rather than viscoelasticity.

Figure 6(d) shows velocity profiles for the viscoelastic fluid in the radial flow region. At the inlet to this region ($R = 1$), the velocity profile is not symmetric about the midplane $Z = 0$. Fluid particles in the upper half of the slit ($1 \le Z \le 0$) move slightly faster than those in the lower half ($0 \le Z \le 1$). Figure 6(b) shows that the axial velocity at the inlet to the radial flow region ($R = 1$) is positive, which indicates that the fluid particles are moving toward the lower disk (i.e., in the positive Z-direction). The radial velocity profile becomes essentially symmetric at $R^{-1} < 0.79$ (somewhat downstream from the corner) in Figure 6(d), and then agrees with the GNF prediction in Figure 5(d), which is nearly the same as the power-law analytic solution.

The radial pressure gradient in the radial flow region is shown in Figure 6(e). At large R (i.e., far from the corner), the profile agrees with the GNF result in Figure 5(a), and is surprisingly well approximated by the power-law analytic solution obtained by Laurencena and Williams (1974). However, at small R, the MZFD pressure gradient is higher than the GNF prediction and is not symmetric about $Z = 0$. Such an increase in the pressure was predicted qualitatively in the work by Lee and Williams (1976a) for an Oldroyd model and in the perturbation analysis by Co and Bird (1977) for the third-order fluid.

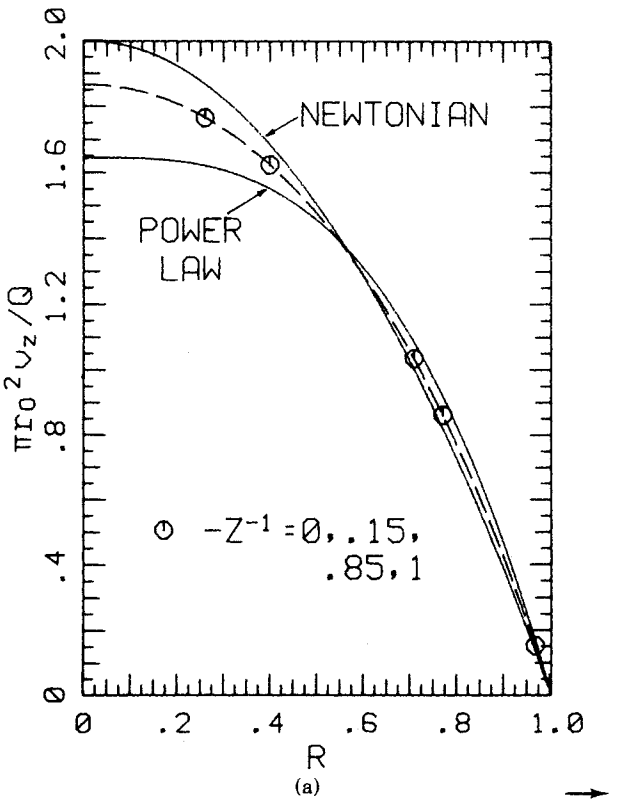

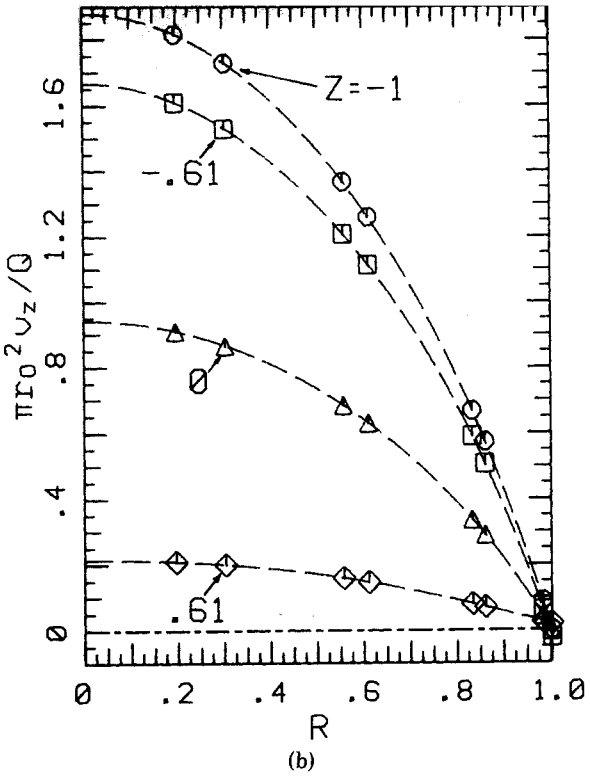

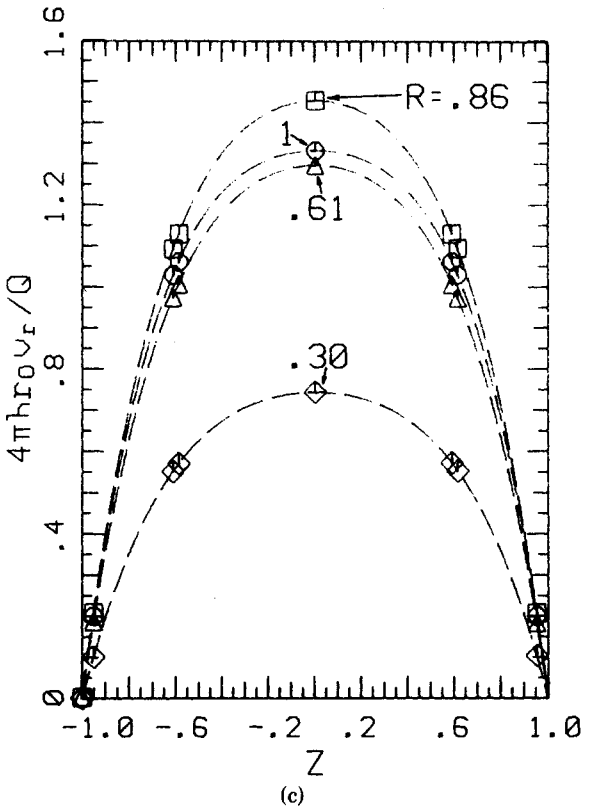

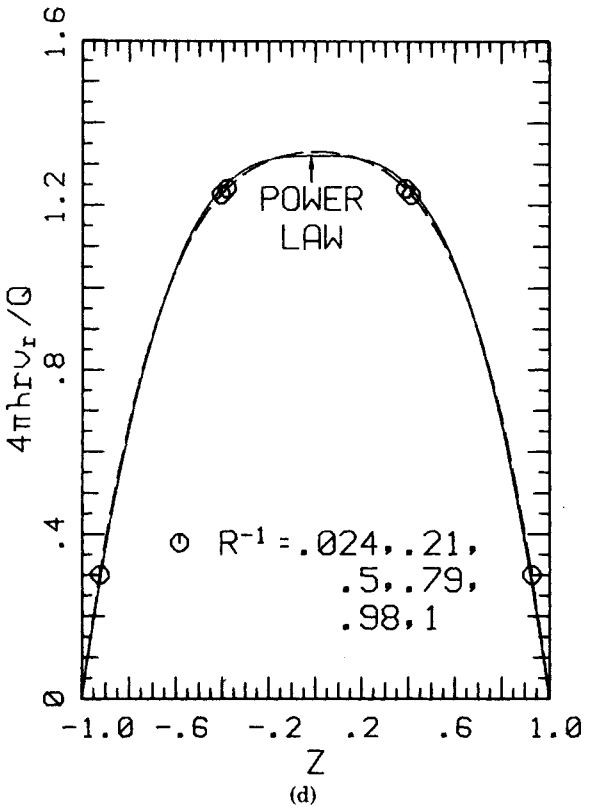

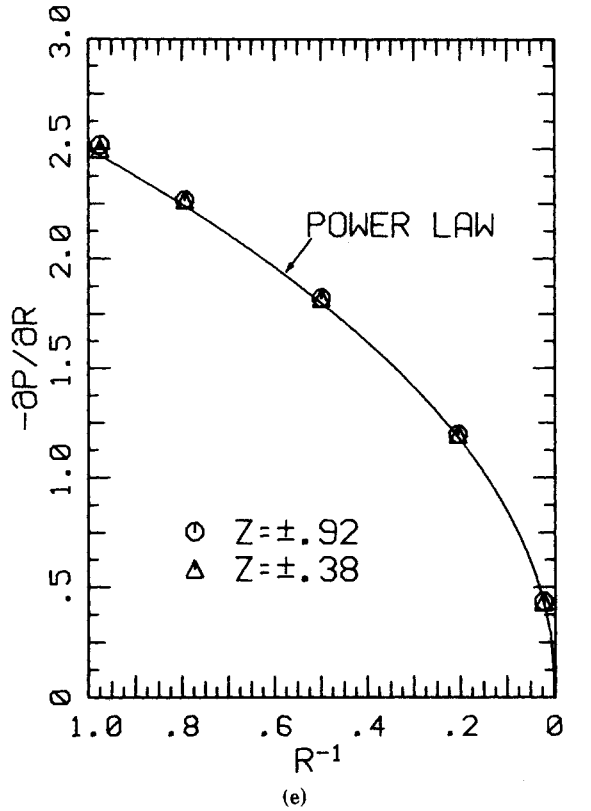

Figure 5. Results for Generalized Newtonian Fluid (inelastic) with Λ_v = 817.7 and n = 0.4741 at Re = 1.096 × 10^{-3} and R_0 = 60. *NRT*1 = 3, *NRT*3 = 5, *NZT*1 = 3, and *NZT*3 = 4. (a) Axial velocity profiles in tube flow region. (b) Axial velocity profiles in stagnation flow region. (c) Radial velocity profiles in stagnation flow region. (d) Radial velocity profiles in radial flow region. (e) Radial pressure gradient profiles in radial flow region. Symbols designate collocation points; dashed lines represent collocation polynomials.

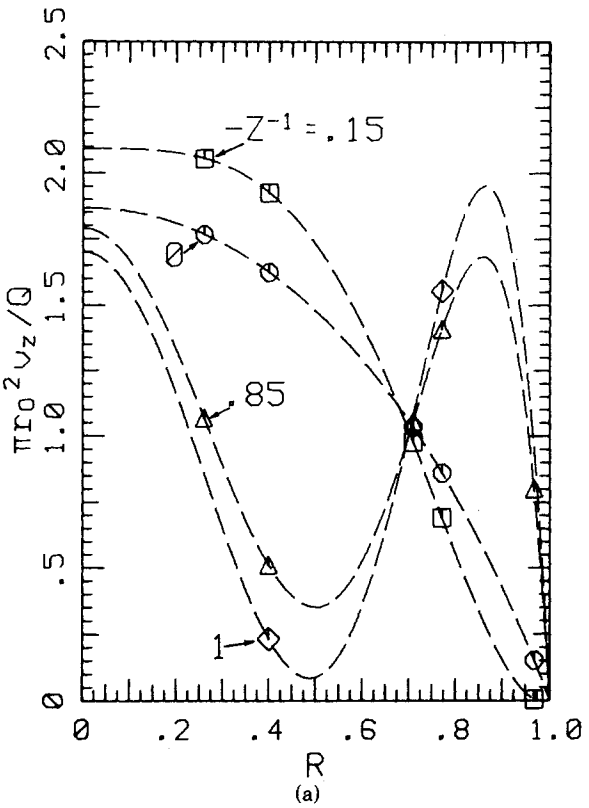

(a)

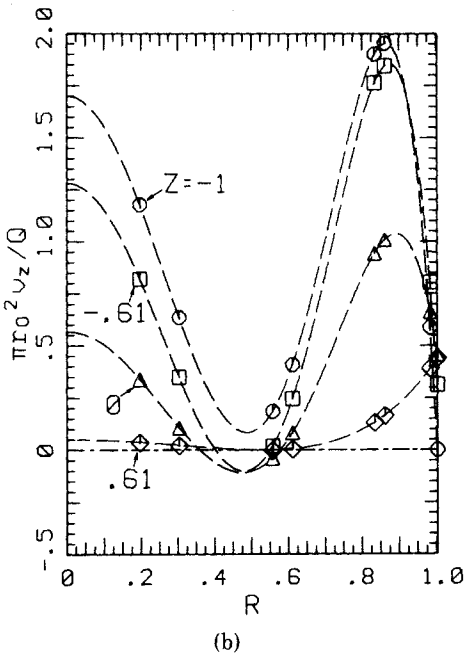

(b)

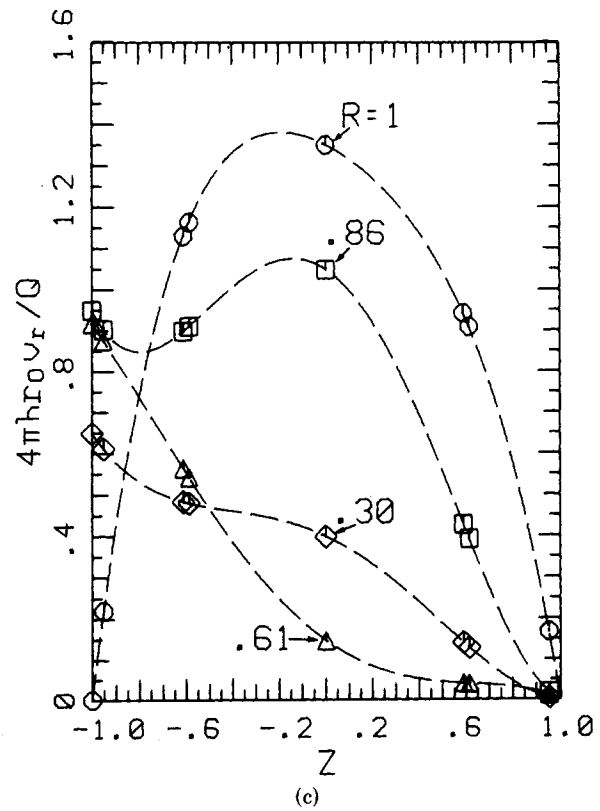

(c)

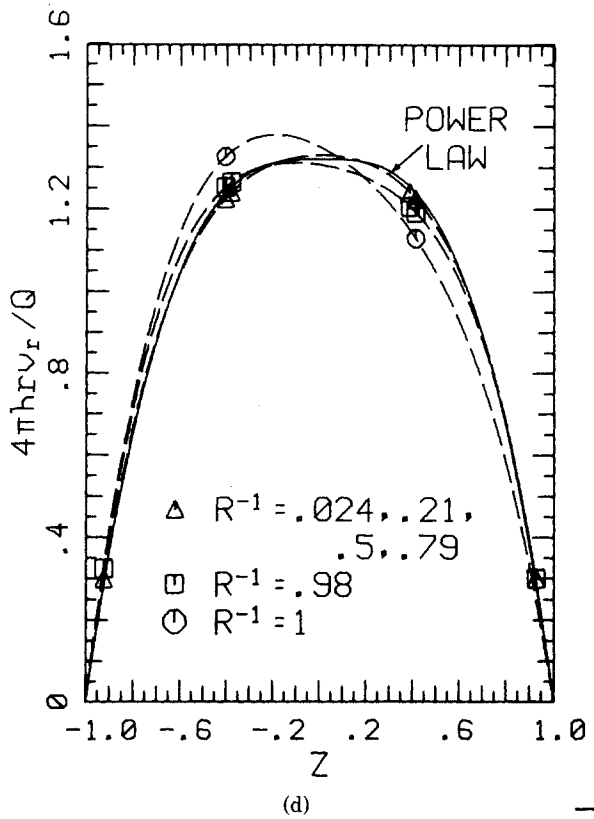

(d)

The shear rates at various locations for the MZFD model calculations are shown in Table 12. The shear rates in most parts of the flow system, except for $Z^{-1} > -0.146$ in the tube, are greater than $0.1s^{-1}$. In Figure 2 the region with $\dot{\gamma} > 0.1s^{-1}$ corresponds to the power-law region of the λ curve. Hence, the value of λ_0 is unimportant here. In Table 12 the shear rate is highest at the point $R^{-1} = 0.976$ and $Z = -0.924$ of the radial flow region. This high shear rate ($\dot{\gamma} = 39.2s^{-1}$) corresponds to an elongation rate ($\dot{\epsilon} = \dot{\gamma}/\sqrt{3}$) of $22.6s^{-1}$. Referring to Figure 3, we can see that this is below the region ($\dot{\epsilon} > 30s^{-1}$) that shows an upturn of the $\bar{\eta}/\eta_0$ prediction.

As shown in Figures 5(e) and 6(e), the predicted $\partial P/\partial R$ profiles for the viscoelastic fluid and the generalized Newtonian fluid are very similar for $R^{-1} < 0.8$, i.e., for $r > 1.25\, r_0$. To investigate this

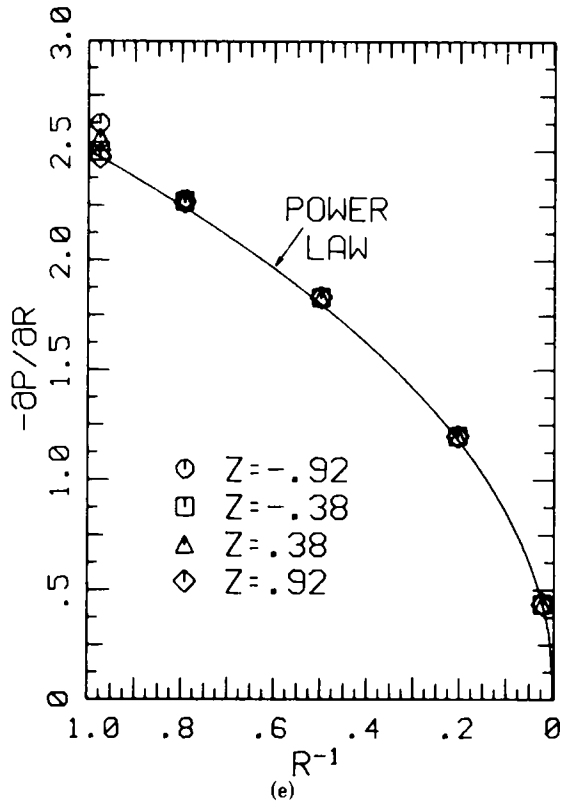

(e)

Figure 6. Results for *MZFD* Model (viscoelastic) with Λ_v = 817.7, n = 0.4741, Λ_t = 592.0, and $\bar{n}$ = 0.423 at Re = 1.096×10^{-3} and R_0 = 60. *NRT*1 = 3, *NRT*3 = 5, *NZT*1 = 3, and *NZT*3 = 4. (a) Axial velocity profiles in tube flow region. (b) Axial velocity profiles in stagnation flow region. (c) Radial velocity profiles in stagnation flow region. (d) Radial velocity profiles in radial flow region. (e) Radial pressure gradient profiles in radial flow region. Symbols designate collocation points; dashed lines represent collocation polynomials.

further, we now examine the fluid system characteristic times. By integrating the inverse of the average velocity $\langle v_r \rangle$ $(= Q/4\pi hr)$ in the radial flow region with respect to r, we find that the average time for a fluid particle to move from the tube radius r_0 to the disk radius r_1 is

$$t_{avg} = 2\pi h(r_1^2 - r_0^2)/Q \tag{28}$$

With Q = 1.117 cm³/s, h = 0.052 cm, r_0 = 3.12 cm and r_1 = 30.48 cm [these are actual experimental conditions from Lee (1974) and are used in generating Figure 6], the average time is 268.9 s. However, the fluid characteristic time lies between 0.02 s and 1.5 s (Figure 2 and Table 12). Since the characteristic radial passage time is much larger than the fluid characteristic time, one would not expect significant elastic effects in the radial flow region as a whole. On the other hand, the passage time from R^{-1} = 1 to R^{-1} = 0.975 (slightly downstream from the corner) is only 0.15 s; thus the deviations from the GNF results in this region [(Figures 5(e) and 6(e)] are plausibly attributed to elasticity.

In the experiments by Lee and Williams (1976b), the total stresses $(p + \tau_{zz})$ at various radial positions of the lower disk were measured with a movable, flush-mounted, strain gauge pressure transducer. Figure 7 shows the pressure data reported by Lee (1974) for the same flow conditions as in Figure 6(e), together with the MZFD, GNF, and power-law predictions. The MZFD and GNF predictions are indistinguishable, but are slightly higher than the analytical power-law solution that neglected entrance effects. The experimental data are higher than our model predictions. The disagreement may be due to: (a) some systematic errors in the experiments (we are reluctant to criticize experimental data from another laboratory since we are not familiar with the operation of their equipment); (b) possible inadequacy of the MZFD model to describe flow near the corner; or (c) some hydrodynamic effects

TABLE 12. TYPICAL SHEAR RATES AT SELECTED POINTS FOR MZFD MODEL

Tube Flow Region

	R		
Z^{-1}	0.259	0.707	0.966
0	0.00925	0.0308	0.0502
−0.146	0.0299	0.0378	0.0148
−0.854	1.647	0.950	1.390

Stagnation Flow Region

	R			
Z	0.195	0.556	0.832	0.981
−0.951	6.30	8.27	10.9	31.4
−0.588	1.09	8.99	2.74	13.7
0	2.14	4.19	4.59	3.37
0.588	5.44	0.272	13.1	16.4
0.951	0.633	2.40	3.44	27.3

Radial Flow Region

	R^{-1}				
Z	0.976	0.794	0.500	0.206	0.0245
−0.924	39.2	29.8	18.9	7.76	0.0245
−0.383	4.50	4.68	2.88	1.21	0.145
0.383	5.57	4.64	2.88	1.21	0.145
0.924	36.3	29.9	18.9	7.76	0.918

These shear rates (in s^{-1}) were the calculated results for *MZFD* model (viscoelastic) with Λ_v = 817.7, n = 0.4741, Λ_0 = 30.50, Λ_t = 592.0, and $\bar{n}$ = 0.423 at Re = 1.096×10^{-3} and R_0 = 60. *NRT*1 = 3, *NRT*3 = 5, *NZT*1 = 3, and *NZT*3 = 4.

which we do not take into account in our modelling. Examples of such effects are flow instabilities, flow in the θ-direction, and dependence of fluid velocity and stresses on the θ-coordinate. At present we cannot explain the discrepancy; more experimental data on this system would be welcome. Viscous heating, which is neglected in this investigation, is not considered as a possible cause for the discrepancy since numerical calculations by Winter (1975)

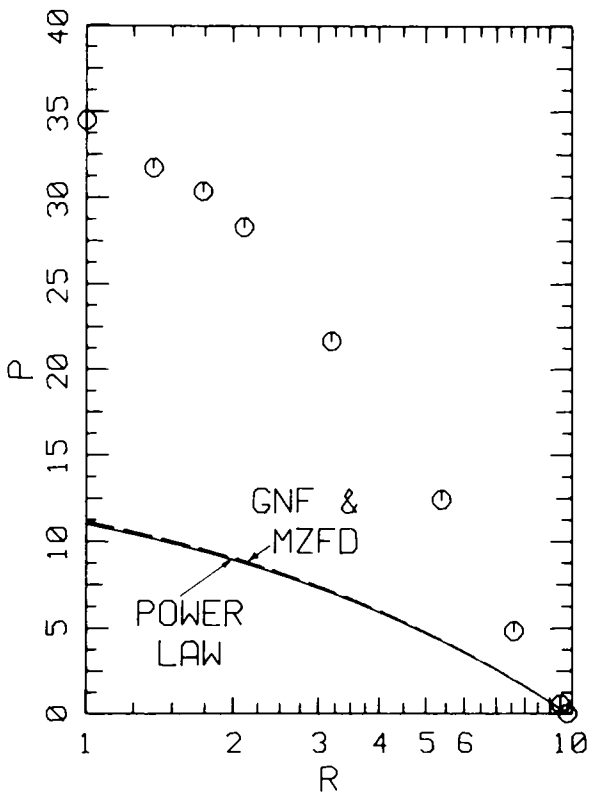

Figure 7. Radial flow pressure profile at the lower disk. The data were reported by Lee (1974) for a Separan solution at Q = 1.117 cm³/s, h = 0.052 cm, r_0 = 3.12 cm, and r_1 = 30.48 cm. These correspond to the flow conditions used in generating Figures 5 and 6. The dashed line represents our *MZFD* and *GNF* predictions; the solid line represents the analytical prediction for a power-law fluid with entrance effects neglected (Laurencena and Williams, 1974).

for a power-law fluid indicate that any temperature increase reduces the pressure gradient.

ACKNOWLEDGMENTS

A. Co wishes to express his gratitude to Professor R. Byron Bird, for his invaluable guidance and encouragement, and to Professors Millard W. Johnson and Arthur S. Lodge, for many helpful and stimulating discussions. For financial support, A. Co is indebted to the National Science Foundation (grant No. ENG-78-06789) and the Vilas Trust Fund of the University of Wisconsin, which provided support under Professor Bird, and to the Research Committee of the Graduate School of the University of Wisconsin at Madison.

NOTATION

$c_{(\ )_{,ij}}$ = adjustable coefficients in the trial functions in Table 8
g = gravity vector
h = half-thickness of the gap between the two disks
i,j = indices
m = constant in power-law viscosity function
M = a dimensionless normal-stress difference, defined in Eq. 13
M_1, M_2, M_3 = trial functions for M in regions 1, 2 and 3, given in Table 8
n = dimensionless exponent in power-law and Carreau viscosity function (Eq. 6); degree of a polynomial
$\bar{n}$ = dimensionless exponent in fluid characteristic time function (Eq. 7)
N = a dimensionless normal-stress difference, defined in Eq. 14
N_1, N_2, N_3 = trial functions for N in regions 1, 2 and 3, given in Table 8
$NRT1, NRT3 \ldots$ = integer parameters defined in Table 9
p = pressure
P = dimensionless modified pressure defined in Eq. 23
P_3 = trial function for P in region 3, given in Table 8
$\mathcal{P}$ = modified pressure, defined by $\mathcal{P} = p - \rho \boldsymbol{g}\cdot\boldsymbol{r}$
Q = volumetric flow rate in the radial flow system
r = radial coordinate
r_0 = inner radius of circular tube connected to the upper disk
r_1 = outer radius of the disks
$\boldsymbol{r}$ = position vector
R = dimensionless radial position, r/r_0
R_0 = geometric ratio, r_0/h
Re = Reynolds number defined in Eq. 19
T = dimensionless shear stress, defined in Eq. 12
T_1, T_2, T_3 = trial functions for T in regions 1, 2 and 3, given in Table 8
$T_n(x)$ = Tschebysheff polynomial of degree n in x
$T_n^*(x)$ = shifted Tschebysheff polynomial of degree n in x
$\boldsymbol{v}$ = velocity vector with components v_i
x = independent variable in a polynomial
z = axial coordinate
Z = dimensionless axial position, z/h

Greek Symbols

$\dot{\gamma}$ = $\sqrt{(1/2)(\dot{\boldsymbol{\gamma}}:\dot{\boldsymbol{\gamma}})}$, a scalar invariant of $\dot{\boldsymbol{\gamma}}$
$\dot{\boldsymbol{\gamma}}$ = rate-of-deformation tensor, $\nabla \boldsymbol{v} + (\nabla \boldsymbol{v})^\dagger$, with components $\dot{\gamma}_{ij}$
$\dot{\Gamma}$ = dimensionless measure of $\dot{\gamma}$, defined in Eq. 15
$\dot{\epsilon}$ = elongational rate
η = viscosity function, defined in Eq. A of Table 3
η_0 = zero-shear-rate viscosity
η^+ = shear stress growth function, defined in Eq. D of Table 3
η^- = shear stress relaxation function, defined in Eq. G of Table 3
$\bar{\eta}$ = elongational viscosity, defined in Eq. J of Table 3
$\bar{\eta}^+$ = elongational stress growth function, defined in Eq. K of Table 3
H = dimensionless viscosity function, η/η_0
θ = tangential coordinate
λ = fluid characteristic time
λ_0, λ_t = time constants in fluid characteristic time function (Eq. 7)
λ_v = time constant in the Carreau viscosity function (Eq. 6)
Λ = dimensionless fluid characteristic time, defined in Eq. 17
$\Lambda_0, \Lambda_t, \Lambda_v$ = dimensionless time constants (corresponding to λ_0, λ_t, λ_v), defined in Eqs. 20, 21, 22
ρ = fluid density
$\boldsymbol{\tau}$ = extra stress tensor with components τ_{ij}
$\phi_i(x)$ = basis function of order i in x (Eqs. 26 and 27)
ψ = stream function, defined in Eqs. 1 and 2
Ψ = dimensionless stream function, defined in Eq. 10
Ψ_1, Ψ_2 = primary and secondary normal-stress coefficients, defined in Eqs. B and C of Table 3
Ψ_1^+, Ψ_2^+ = primary and secondary normal-stress growth function, defined in Eqs. E and F of Table 3
Ψ_1^-, Ψ_2^- = primary and secondary normal-stress relaxation functions, defined in Eqs. H and I of Table 3
$\Psi_1^o, \Psi_2^o, \Psi_3^o$ = known functions in Eq. 24 for regions 1, 2 and 3 (Table 8)
$\Psi_1^c, \Psi_2^c, \Psi_3^c$ = functions in Eq. 24 for regions 1, 2 and 3 (Table 8)
ω = $\partial v_r/\partial z - \partial v_z/\partial r$, θ-component of the vorticity vector $[\nabla \times \boldsymbol{v}]$
$\boldsymbol{\omega}$ = vorticity tensor, $\nabla \boldsymbol{v} - (\nabla \mathrm{v})^\dagger$
Ω = dimensionless measure of ω, defined in Eq. 11

Mathematical Operations

∇ = "del" operator
D/Dt = substantial derivative, $\partial/\partial t + \boldsymbol{v}\cdot\nabla$
$\mathcal{D}(\ )/\mathcal{D}t$ = corotational or Jaumann derivative, $D(\ )/Dt + (1/2)\{\boldsymbol{\omega}\cdot(\ ) - (\ )\cdot\boldsymbol{\omega}\}$
Σ = summation symbol
$\langle\ \rangle$ = average over a flow cross section

Superscripts

^{o} = reference value
† = transpose of a tensor

LITERATURE CITED

Amadou, H., P. M. Adler, and J. M. Piau, "Converging Radial Flow of Dilute Polymer Solution," *J. Non-Newtonian Fluid Mech.*, **4**, 229 (1978).

Bird, R. B., R. C. Armstrong and O. Hassager, *Dynamics of Polymeric Liquids, Volume 1: Fluid Mechanics*, Wiley, New York (1977).

Bird, R. B., W. E. Stewart and E. N. Lightfoot, *Transport Phenomena*, Wiley, New York (1960).

Carreau, P. J., "Rheological Equations from Molecular Network Theories," Ph.D. Thesis, University of Wisconsin, Madison (1968).

Chang, P.-W., T. W. Patten and B. A. Finlayson, "Collocation and Galerkin Finite Element Methods for Viscoelastic Fluid Flow. Part I—Description of Method and Problems with Fixed Geometry. Part II—Die Swell Problems with a Free Surface," *Computers and Fluids*, **7**, 267, 285 (1979).

Co, A., "Viscoelastic Radial Flow between Parallel Disks," Ph.D. Thesis, University of Wisconsin, Madison (1979).

Co, A., "Inelastic Flow from a Tube into a Radial Slit," *Ind. Eng. Chem. Fundam.*, **20** (1981).
Co, A., and R. B. Bird, "Slow Viscoelastic Radial Flow between Parallel Disks," *Appl. Sci. Res.*, **33**, 385 (1977).
Criminale, W. O. Jr., J. L. Ericksen and G. L. Filbey, Jr., "Steady Shear Flow of Non-Newtonian Fluids," *Arch. Rat. Mech. Anal.*, **1**, 410 (1958).
Curtiss, C. and R. B. Bird, "A Kinetic Theory for Polymer Melts. Part I: The Equation for the Single-Link Orientational Distribution Function. Part II: The Stress Tensor and the Rheological Equation of State," *J. Chem. Phys.*, **74**, 2016 (1981).
DeWitt, T. W., "A Rheological Equation of State which Predicts Non-Newtonian Viscosity, Normal Stresses and Dynamic Moduli," *J. Appl. Phys.*, **26**, 889 (1955).
Doi, M. and S. F. Edwards, "Dynamics of Concentrated Polymer Systems. Part 4—Rheological Properties," *J. C. S. Faraday II*, **75**, 38 (1979).
Ericksen, J. L., "The Behavior of Certain Viscoelastic Materials in Laminar Shearing Motions," in *Viscoelasticity: Phenomenological Aspects*, J. T. Bergen (ed.), Academic Press, New York (1960).
Finlayson, B. A., *The Method of Weighted Residuals and Variational Principles*, Academic Press, New York (1972).
Fromm, H., "Laminare Strömung Newtonscher und Maxwellscher Flüssigkeiten," *Zeits. für angew. Math. u. Mech.*, **25/27**, 146 (1947); **28**, 43 (1948).
Guertin, E. W., J. P. Sørensen and W. E. Stewart, "Exponential Collocation of Stiff Reactor Models," *Computers and Chemical Engineering*, **1**, 197 (1977).
Holstein, H. and D. J. Paddon, "Extrusion Flow between Parallel Plates," *Rheology, Volume 2: Fluids*, G. Astarita, G. Marrucci, and L. Nicolais (eds.), Plenum Press, New York (1980).
Lanczos, C., *Applied Analysis*, Prentice-Hall, Englewood Cliffs, NJ (1956).
Laurencena, B. R. and M. C. Williams, "Radial Flow of Non-Newtonian Fluids between Parallel Plates," *Trans. Soc. Rheol.*, **18**, 331 (1974).
Lee, M. C. H., M. S. Thesis, University of California, Berkeley (1974).
Lee, M. C. H. and M. C. Williiams, "Radial Flow of Viscoelastic Liquids, Part I: Theoretical," *J. Non-Newtonian Fluid Mech.*, **1**, 323 (1976a).
Lee, M. C. H. and M. C. Williams, "Radial Flow of Viscoelastic Liquids, Part II: Experimental," *J. Non-Newtonian Fluid Mech.*, **1**, 343 (1976b).
Nirschl, J. P., "Orthogonal Collocation Analysis of Viscoelastic Fluid Flow in the Disk and Cylinder System," Ph.D. Thesis, University of Wisconsin, Madison (1971).
Pearson, G. and S. Middleman, "Elongational Flow Behavior of Viscoelastic Liquids: Part I. Modeling of Bubble Collapse; Part II. Definition and Measurement of Apparent Elongational Viscosity," *AIChE J.*, **23**, 714 (1977).
Piau, J. M. and M. Piau, "L'écoulement radial laminaire, stationnaire, d'un fluide simple entre deux disques parallèles," *Comptes Rendus Acad. Sci. Paris (A)*, **269**, 1214 (1969).
Piau, J. M. and M. Piau, "L'écoulement radial laminaire, stationaire entre deux disques parallèles, et la mesure du temps caractéristique d'un fluide simple," *Comptes Rendus Acad. Sci. Paris (A)*, **270**, 159 (1970).
Ralston, A., *A First Course in Numerical Analysis*, McGraw-Hill, New York (1965).
Schwarz, W. H. and C. Bruce, "The Radial Flow Viscometer," *Chem. Eng. Sci.*, **24**, 399 (1969).
Sørensen, J. P., "Solution of Transport Problems by Use of Trial Function Techniques," Ph.D. Thesis, University of Wisconsin, Madison (1972).
Sørensen, J. P., E. W. Guertin and W. E. Stewart, "Computational Models for Cylindrical Catalyst Particles," *AIChE J.*, **19**, 969, 1286; **21** 206 (1975) (1973).
Sørensen, J. P., M. S. Willis, and W. E. Stewart, "Effects of Column Asymmetry on Thermal Diffusion Separations," *J. Chem. Phys.*, **59**, 2676 (1973).
Sørensen, J. P. and W. E. Stewart, "Computation of Forced Convection in Slow Flow through Ducts and Packed Beds—Parts I to IV," *Chem. Eng. Sci.*, **29**, 811 (1974).
Stewart, W. E., J. P. Sørensen, and B. C. Teeter, "Pulse-Response Measurement of Thermal Properties of Small Catalyst Pellets," *Ind. Eng. Chem. Fund.*, **17**, 221 (1978); **18**, 438 (1979).
Villadsen, J. V. and M. L. Michelsen, *Solution of Differential Equation Models by Polynomial Approximation*, Prentice-Hall, Englewood Cliffs, NJ (1978).
Villadsen, J. V. and W. E. Stewart, "Solution of Boundary-Value Problems by Orthogonal Collocation," *Chem. Eng. Sci.*, **22**, 1483 (1967); **23**, 1515 (1968).
Winter, H. H., "Approximate Calculation and Measurement of the Pressure Distribution in Radial Flow of Molten Polymers between Parallel Discs," *Polym. Eng. Sci.*, **15**, 460 (1975).
Woolard, H. W., "A Theoretical Analysis of the Viscous Flow in a Narrowly Spaced Radial Diffuser," *J. of Appl. Mechanics*, **24**, 9, 644 (1957).
Zaremba, S., "Sur une forme perfectionneé de la theorie de la relaxation," *Bull. Int. Acad. Sci. Cracovie*, 594 (1903).
Zaremba, S., "Le principe des mouvements relatifs et les équations de la mécanique physique," *Bull. Int. Acad. Sci. Cracovie*, 614 (1903).

Manuscript received October 27, 1980, revision received August 24, and accepted August 31, 1981.